Suplemento de la Revista Mexicana de Física 3 040904 (2022) 1–6

Determination of the shear viscosity and light quark diffusivity of QGP with two-particle correlation functions

Claude Pruneau
Department of Physics and Astronomy, Wayne State University, Detroit, 48201, USA

Received 3 July 2022; accepted 15 September 2022

We discuss measurements of general balance functions recently reported by the ALICE collaboration in the context of a two-stage quark production model and towards the determination of light quark diffusivity.

1 Introduction and Historical Context

Studies heavy ion collisions at RHIC and LHC over the last two decades have established strong evidence a form of matter akin to a Quark Gluon Plasma (QGP) is formed in these collisions [1–19]. The experimental focus, both at RHIC and LHC, has thus in part shifted to high precision measurements of the properties of this new form of matter. Although recent measurements have largely targeted a precise determination of the specific shear and bulk viscosity of QGP matter, it is important to remind ourselves that several other properties are of interest, including the matter compressibility, its (electric and color) conductivity, heat capacity, quark diffusivity, stopping power, as well as susceptibilities. It is also of interest to further our understanding of the collision dynamics, the system evolution, and characteristics of the QGP/Hadron phase transition. Nominally, several of these properties might be accessible via measurements of integral and differential correlation functions. In this presentation, I focus on measurements of balance functions recently reported by the ALICE collaboration towards the observation of two stages quark production as well as the determination of the light quark diffusivity.

Measurements of balance functions were introduced more than 20 years ago by Pratt et al. [20, 21] as a technique to establish the presence of delayed hadronization in heavy ion collisions. On expects that a large number of quarks (q), anti-quarks ($\bar{q}$), and gluons (g) are created and quickly form a hot and dense fireball at the onset of collisions between two large Lorentz contracted nuclei. The fireball then rapidly expands based on internal pressure gradients along the beam direction (longitudinal expansion), the collision impact parameter, $\bar{b}$, and outside of the collision plane, thereby also yielding anisotropic particle production in the transverse plane. Being rapid, the expansion is expected to proceed isentropically until the system temperature becomes too low to sustain a QGP phase. At that time, gluons collisions yield additional $q\bar{q}$ pairs creation and hadrons eventually form and freeze out.

The late stage of quark production takes place at much lower temperature than the initial stage. Charge balancing $q\bar{q}$ pairs produced at early times thus feature large rapidity differences (Δy) in part as a result of the fast longitudinal expansion and in part as a result of the large $\sqrt{s}$ characterizing their production at the onset of collisions. On the other hand, $q\bar{q}$ produced at the latter stage are characterized by a smaller $\sqrt{s}$ and thus feature, on average, much smaller rapidity differences. Given late stage production of strange anti-strange ($s\bar{s}$) pairs is suppressed relative to the creation of the much lighter $u\bar{u}$ and $d\bar{d}$, one expects that charge balancing K^+ and K^- pairs have broad longitudinal correlations originating at early times. But by contrast, charge balancing pions (π^+ and π^-) have longitudinal correlations determined by the relative proportion of early and late stage production of $u\bar{u}$ and $d\bar{d}$ pairs. Peripheral collisions produce small size fireballs and their charge balancing correlation functions are expected to be dominated by early emission whereas central collisions feature a large fireball that yields a strong late stage emission of light quarks. One consequently expects that charge balancing pion correlation functions, known as balance functions (BFs), are wide in peripheral collision but longitudinally narrow in central collisions whereas the width of kaon BFs are approximately independent of the collision centrality given they are predominantly formed from $s\bar{s}$ pairs produced at the onset of collisions.The main initial goal of measurements of balance functions was thus to find out whether pions and kaons feature balance functions that exhibit different evolution with collision centrality.

Measurements of charge balance functions were first completed by the STAR experiment in Au – Au collisions and showed that longitudinal pion balance functions narrow significantly from peripheral to central collisions whereas those of kaons exhibit little dependence, if any, on the collision centrality, thereby supporting the notions of two stage quark production and delayed hadronization [22–25]. Measurements of inclusive charge balance functions performed by the ALICE collaboration in Pb – Pb collisions showed a significant narrowing from peripheral to central collisions for $0.15 < p_{\mathrm{T}} < 2.0$ GeV/c charged hadrons and essentially constant balance function widths for higher p_{T} particles also supporting the notion that the longitudinal balance function of pions should narrow with increasing collision centrality [26, 27]. It was then imperative to also measure identified balance functions of identified hadrons, specifically those of pions and ka ons. However, in parallel with these developments, it is also emerged that the azimuthal width of balance functions might have good sensitivity to the diffusivity of light quarks. Pratt et al. in fact showed the sensitivity to light quark diffusivity should grow with the hadron mass, i.e., kaons and protons BFs should afford better sensitivity to the diffusivity than pions [28, 29]. It then became of interest to measure general balance functions, i.e., balance functions of all identifiable charged light hadrons.

In this talk, I present a summary of recent measurements of general balance functions of identified charged pions, kaons, and protons and their anti-particles by the ALICE collaboration [30, 31]. The definition of general balance functions and the methodology used by the ALICE collaboration to measure them are introduced in sec. II, whereas the results are presented in sec. III. Section IV discusses the results in light of predictions of the light quark diffusivity by LQCD [32].

2 General Balance Function Definition

General balance functions are defined as an extension of the original balance function introduced by Pratt et al. [**?**]. Nominally expressed as differences of conditional densities defined as functions of the rapidities y_i and azimuthal angles φ_i, of the particles $i = 1, 2$ composing a pair, the ALICE measurement focuses on the $\Delta y = y_1 - y_2$ and $\Delta\varphi = \varphi_1 - \varphi_2$ dependence of the correlations and averages out the $\bar{y} = (y_1 + y_2)/2$ and $\bar{\varphi} = (\varphi_1 + \varphi_2)/2$ dependence across the acceptance of the ALICE TPC

$$B_2^{\alpha\beta}(\Delta y, \Delta\varphi) = \frac{1}{2}\left[\frac{\rho_2^{\alpha\bar{\beta}}(\Delta y, \Delta\varphi)}{\rho_1^{\bar{\beta}}} - \frac{\rho_2^{\bar{\alpha}\bar{\beta}}(\Delta y, \Delta\varphi)}{\rho_1^{\bar{\beta}}} + \frac{\rho_2^{\bar{\alpha}\beta}(\Delta y, \Delta\varphi)}{\rho_1^{\beta}} - \frac{\rho_2^{\alpha\beta}(\Delta y, \Delta\varphi)}{\rho_1^{\beta}}\right], \tag{1}$$

in which ρ_1^{α} and $\rho_2^{\alpha\beta}$ are single and pair densities, respectively, for particles of type α and β. Bar labels, $\bar{\alpha}$, $\bar{\beta}$ are used to denote anti-particles. However, to suppress dependencies on detection efficiencies, the measurement was performed in terms of robust normalized cumulants R_2 according to

$$B_2^{\alpha\beta}(\Delta y, \Delta\varphi) \approx \frac{1}{2}\left[\rho_1^{\bar{\alpha}} R_2^{\alpha\bar{\beta}} - \rho_1^{\bar{\alpha}} R_2^{\bar{\alpha}\bar{\beta}} + \rho_1^{\bar{\alpha}} R_2^{\bar{\alpha}\beta} - \rho_1^{\alpha} R_2^{\alpha\beta}\right], \tag{2}$$

where

$$R_2^{\alpha\beta} = \frac{\rho_2^{\alpha\beta}(\Delta y, \Delta\varphi)}{\rho_1^{\alpha} \otimes \rho_1^{\beta}(\Delta y, \Delta\varphi)} - 1. \tag{3}$$

Eq. (2) becomes exact in the limit $\rho_1^{\bar{\alpha}} = \rho_1^{\alpha}$ encountered at the LHC.

3 Experimental Methods

The balance function measurements were carried out with the ALICE detector whose design, performance, and operation were reported elsewhere [**?**, **?**]. The analysis is based on $\sqrt{s_{\rm NN}}$ =2.76 TeV Pb–Pb collision data accumulated during the 2010 LHC run with a minimum bias trigger. Collisions are partitioned in collision centrality classes based on energy deposited in the V0A and V0C detectors. Charged particles are momentum analyzed with the TPC and species identified based on their energy losses in the TPC gas and their velocity measured with the time-of-flight (TOF) detector. See the main ALICE main paper reporting this analysis for detailed discussions of corrections, event and track quality cuts, purity, etc [31].

4 Results

Balance functions (BF) of nine species pairs, $\pi\pi$, πK, πp, $K\pi$, . . ., pp were measured as functions of Δy, $\Delta\varphi$ and for selected collision centrality ranges. The three examples displayed Fig. 1 illustrate the main features of measured BFs: a prominent near side peak centered at Δy, $\Delta\varphi = 0$ and an approximately flat away-side ($\Delta\varphi = \pi$). These features are understood to result in large part from the collision system's large radial velocity. Figures 2, 3 display projections on the nine measured BFs onto the Δy, $\Delta\varphi$ axes, respectively. Although somewhat similar, these BF projections feature distinct shapes and evolution with collision centrality. Note that the BFs of $\pi\pi$, $K\pi$, and πp and exhibit the strongest dependence on collision centrality whereas KK and pp BFs shows negligible evolution with centrality. Collision centrality dependencies are best characterized by the longitudinal and azimuthal rms widths, $\sigma_{\Delta y}$ and $\sigma_{\Delta\varphi}$ of these distributions shown in Fig. 4. In the azimuthal direction, all nine BFs significantly narrow from peripheral to central collisions as a result of the large radial flow present in more central collisions. One notes, however, that the actual $\Delta\varphi$ widths and rate of decrease with centrality vary for the nine pairs of species. In the longitudinal directions, Δy, all species pairs, except KK and pp, show substantial narrowing from peripheral to central collisions whereas KK and pp BFs are essentially independent of collision centrality. This centrality evolution

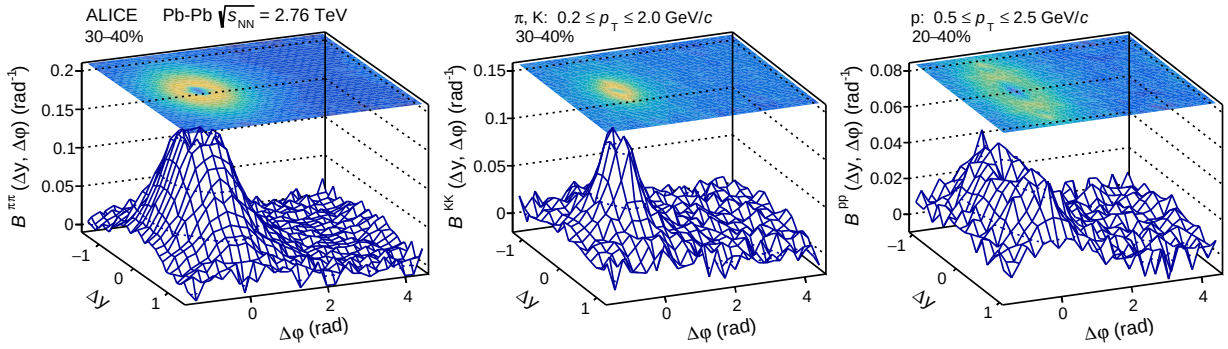

FIGURE 1. Balance functions $B^{\alpha\beta}(\Delta y, \Delta\varphi)$ of pairs $\alpha\beta = \pi\pi$ (left), KK (center), and pp (right) measured in semi-central Pb–Pb collisions at $\sqrt{s_{\rm NN}} = 2.76$ TeV.

difference matches expectations from collision dynamics involving two stages of quark production (delayed hadronization). Note however that the rms width of the pp BF is essentially determined by the width of the acceptance. It is thus difficult to determine how this particular BF truly evolves with collision centrality.

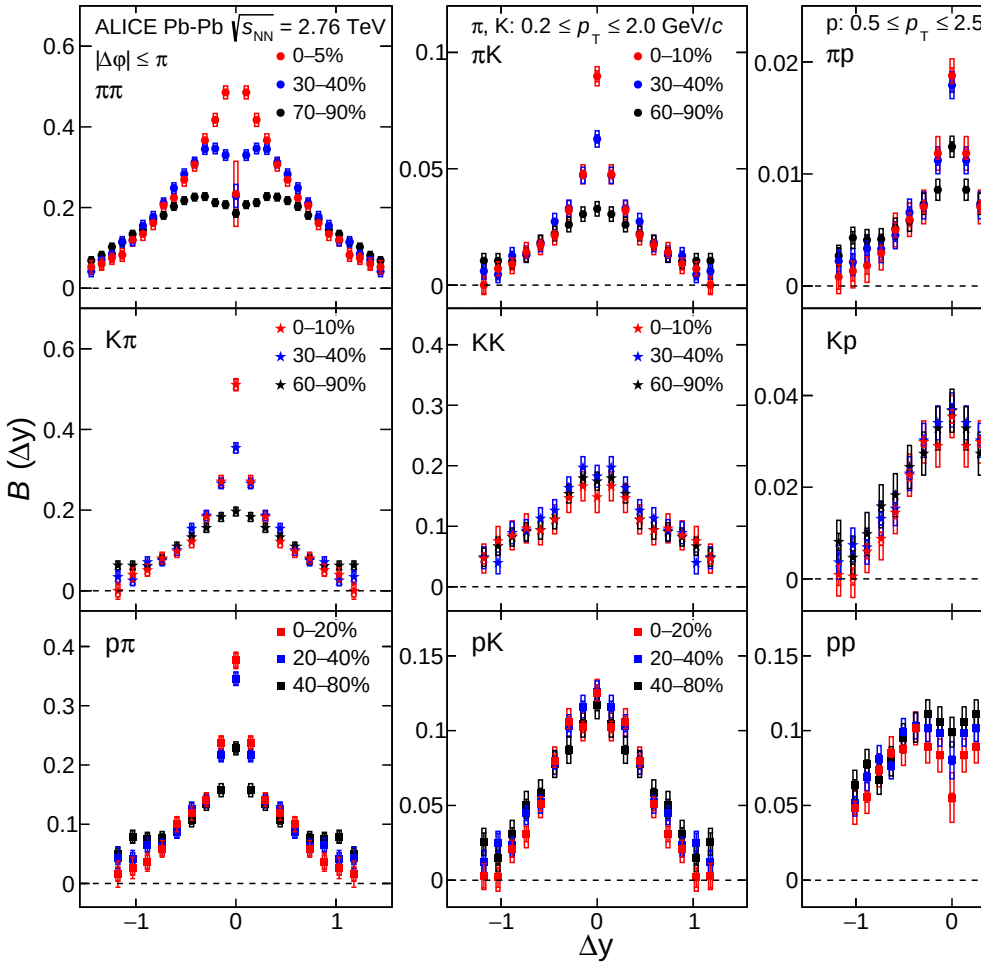

FIGURE 2. Balance function of species pairs $(\pi, \mathrm{K}, \mathrm{p}) \otimes (\pi, \mathrm{K}, \mathrm{p})$ projected onto the Δy axis for particle pairs within the full range $|\Delta\varphi| \leq \pi$. Vertical bars and open boxes represent statistical and systematic uncertainties, respectively.

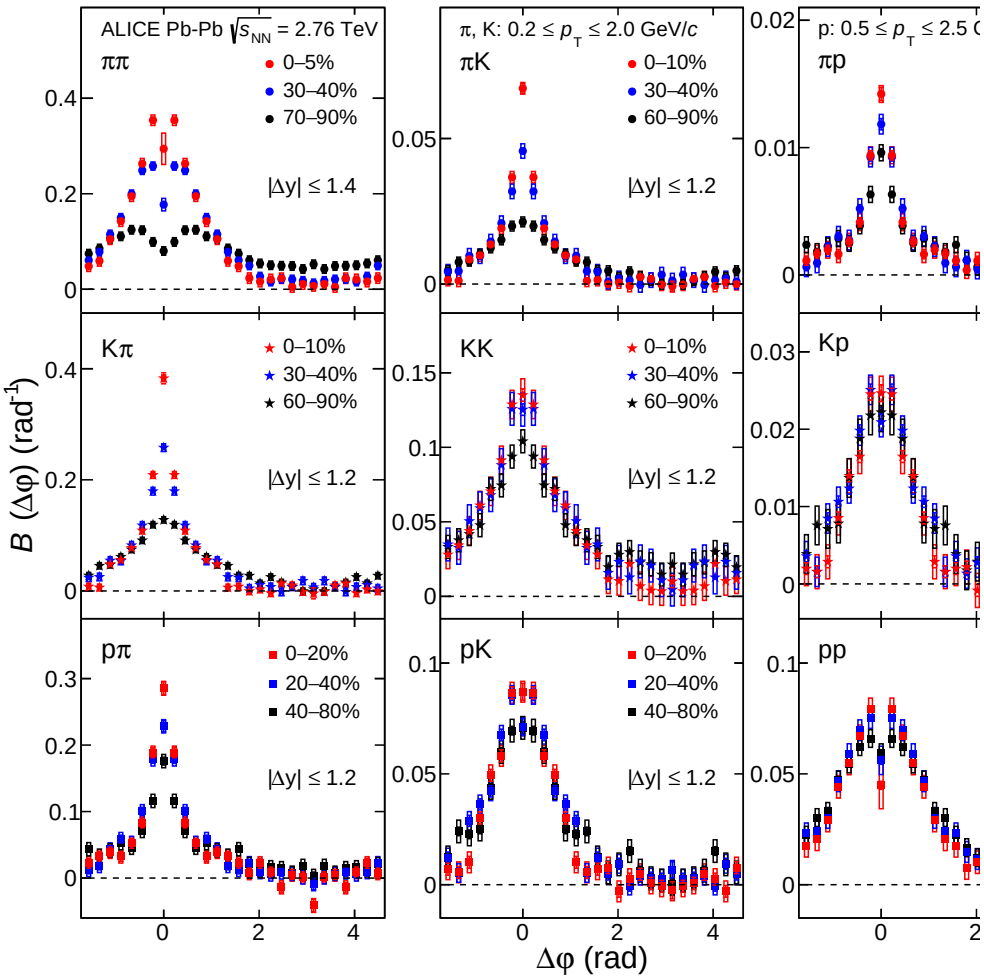

FIGURE 3. Balance function projections of species pairs $(\pi, \mathrm{K}, \mathrm{p}) \otimes (\pi, \mathrm{K}, \mathrm{p})$ onto the $\Delta\varphi$ axis for the different particle pairs. Vertical bars and open boxes represent statistical and systematic uncertainties, respectively.

5 Discussion

Though originally proposed to assess the existence of two stage quark production and delayed hadronization, which is largely supported by the BFs reported in this work, it recently emerged that BFs provide invaluable information about the hadronization stage, particularly the nature of the full hadronic cocktail produced at freeze out, which eventually decay into measurable light hadrons (i.e., π, K, p, $\bar{p}$, etc) [28]. While blastwave fits with feeddown contributions to single particle spectra provide a method to assess the contributions from higher mass states, general BFs and cross species correlation functions provide enhanced precision in the evaluation of the role and importance of these feed-downs. Indeed, to be proven valid, hadron gas models must not only provide feed-down probabilities to specific single particle species, they must also include predictions of the strength and shape of correlated pairs. Particular pairs of species are distinctly populated by high mass hadrons. Having access to integral as well as the shape of BFs thus provide additional insight into the freeze out stage resulting in low mass measurable particles. The lower panel of Fig. 3 displays values of the integral of the BFs of all nine pairs of species. Except for the $\pi\pi$ BF, all other BFs have integrals that are approximately constant (i.e., “invariant") with collision centrality. This suggests that the feeddown processes leading to these correlated pairs have yields that do not vary much with collision centrality. In turn, this suggest that the mass spectrum of hadron states does not vary appreciably in the centrality range examined in this work. Further and more quantitative model studies are evidently required to justify and articulate this statement in greater detail.

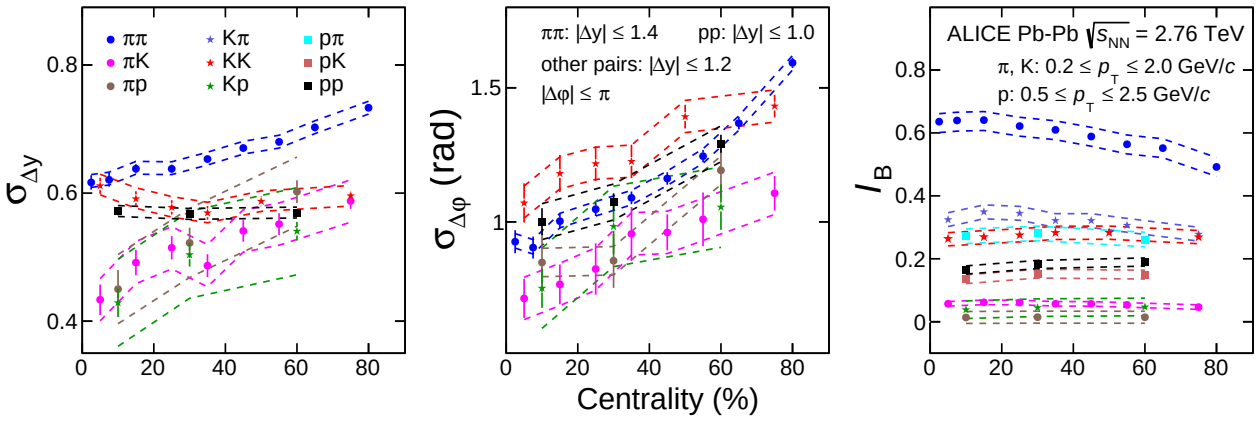

FIGURE 4. Longitudinal (Δy) σ widths (left), azimuthal ($\Delta\varphi$) σ widths (center), and integrals (right) of balance functions of the full species matrix of $\pi^{\pm}$, $K^{\pm}$, and $p/\overline{p}$ with centrality. For Δy and $\Delta\varphi$ widths, $K\pi$, $p\pi$, and pK have the same values with πK, πp, and Kp, respectively. For the longitudinal widths, the relative azimuthal angle range for all the species pairs is the full azimuth range $|\Delta\varphi| \leq \pi$. For the azimuthal widths, the relative rapidity range used for all species pairs is $|\Delta y| \leq 1.2$, with the exception of $|\Delta y| \leq 1.4$ for $\pi\pi$ and $|\Delta y| \leq 1.0$ for pp. Vertical bars represent statistical uncertainties while systematic uncertainties are displayed as dash line bands.

Azimuthal correlations and in particular balance functions have been proposed as a probe of the light quark diffusivity in the QGP phase [**?**,28]. Recently, Pratt et al. compared hydrodynamic calculations that include quark diffusivity of light quarks and scattering of hadrons with preliminary data reported by the ALICE collaboration [29,30]. The calculations were performed with several levels of quark diffusivity corresponding to 1/2, 1, 2, and 4 times the diffusivity predicted by Lattice QCD (LQCD) calculations [32]. It emerged that the ALICE data are best matched by calculations performed with the nominal diffusivity obtained by LQCD but the data are likely compatible also with somewhat smaller or larger values of the diffusivity. The addition of the data recently obtained by the ALICE collaboration and briefly summarized in this work should help, hopefully, to confirm this initial statement and potentially further narrow the range of diffusivity values compatible with measured balance functions.

Measurements of BFs identified species pairs are expected to become more precise and simpler to accomplish with the large datasets recently acquired by the ALICE collaboration as well as those anticipated from LHC runs 2 and 3. There is thus great needs to further improve measurement and correction techniques, on the experimental side, and reach a better understanding of the impact of processes such as radial flow, anisotropic flow, and femtoscopic correlations on the shape and integral of balance functions. Much work remains to be done but efforts should pay off given general balance functions feature good sensitivity to some key properties of the QGP matter produced in A–A collisions.

6 Acknowledgements

This work was supported in part by DOE Grant Number: DE-FG02-92ER40713.

1. J. Adams et al., Experimental and theoretical challenges in the search for the quark gluon plasma: The STAR's critical assessment of the evidence from RHIC collisions, Nucl. Phys. A757 (2005) 102, 10.1016/j.nuclphysa.2005.03.085
2. K. Adcox et al., Formation of dense partonic matter in relativistic nucleus-nucleus collisions at RHIC: Experimental evaluation by the PHENIX, Nucl. Phys. A757 (2005) 184, 10.1016/j.nuclphysa.2005.03.086
3. I. Arsene et al., Quark gluon plasma and color glass condensate at RHIC? The perspective from the BRAHMS experiment, Nuclear Physics A 757 (2005) 1 , http://dx.doi.org/10.1016/j.nuclphysa.2005.02.130
4. B. B. Back et al., The PHOBOS perspective on discoveries at RHIC, Nucl. Phys. A757 (2005) 28, 10.1016/j.nuclphysa.2005.03.084
5. J. Adams et al., Azimuthal anisotropy in Au–Au collisions at $\sqrt{s_{\rm NN}}$ = 200 GeV, Phys. Rev. **C** 72 (2005) 014904, 10.1103/PhysRevC.72.014904
6. U. Heinz and R. Snellings, Collective flow and viscosity in relativistic heavy-ion collisions, Ann. Rev. Nucl. Part. Sci. 63 (2013) 123, 10.1146/annurev-nucl-102212-170540
7. K. Aamodt et al., Elliptic flow of charged particles in Pb-Pb collisions at 2.76 TeV, Phys. Rev. Lett. 105 (2010) 252302, 10.1103/PhysRevLett.105.252302

8. J. Adams et al., Evidence from d + Au measurements for final state suppression of high $p_{\rm T}$ hadrons in Au–Au collisions at RHIC, Phys. Rev. Lett. 91 (2003) 072304, 10.1103/PhysRevLett.91.072304
9. S. Acharya et al., Production of charged pions, kaons, and (anti-)protons in Pb-Pb and inelastic pp collisions at $\sqrt{s_{\rm NN}}$ = 5.02 TeV, Phys. Rev. C 101 (2020) 044907, 10.1103/PhysRevC.101.044907
10. J. Adams et al., Transverse-Momentum and Collision-Energy Dependence of High-p_T Hadron Suppression in Au–Au Collisions at Ultrarelativistic Energies, Phys. Rev. Lett. 91 (2003) 172302, 10.1103/PhysRevLett.91.172302
11. S. S. Adler et al., High-$p_{\rm T}$ charged hadron suppression in Au–Au collisions at $\sqrt{s_{\rm NN}} = 200$ GeV, Phys. Rev. **C** 69 (2004) 034910, 10.1103/PhysRevC.69.034910
12. B. I. Abelev et al., Identified Baryon and Meson Distributions at Large Transverse Momenta from Au–Au Collisions at $\sqrt{s_{\rm NN}} = 200$ GeV, Phys. Rev. Lett. 97 (2006) 152301, 10.1103/PhysRevLett.97.152301
13. J. Adam et al., Measurement of jet suppression in central Pb-Pb collisions at $\sqrt{s_{\rm NN}}$ = 2.76 TeV, Phys. Lett. B 746 (2015) 1, 10.1016/j.physletb.2015.04.039
14. B. B. Abelev et al., Centrality, rapidity and transverse momentum dependence of J/ψ suppression in Pb-Pb collisions at $\sqrt{s_{\rm NN}}$=2.76 TeV, Phys. Lett. B 734 (2014) 314, 10.1016/j.physletb.2014.05.064
15. A. M. Sirunyan et al., Measurement of prompt and nonprompt charmonium suppression in PbPb collisions at 5.02 TeV, Eur. Phys. J. C 78 (2018) 509, 10.1140/epjc/s10052-018-5950-6
16. A. M. Sirunyan et al., Measurement of nuclear modification factors of Υ(1S), Υ(2S), and Υ(3S) mesons in PbPb collisions at $\sqrt{s_{\rm NN}} =$ 5.02 TeV, Phys. Lett. B 790 (2019) 270, 10.1016/j.physletb.2019.01.006
17. S. Acharya et al., Measurement of nuclear effects on $\psi(2{\rm S})$ production in p-Pb collisions at $\sqrt{s_{\rm NN}} = 8.16$ TeV, JHEP 07 (2020) 237, 10.1007/JHEP07(2020)237
18. S. Acharya et al., Centrality and transverse momentum dependence of inclusive J/ψ production at midrapidity in Pb–Pb collisions at $\sqrt{s_{\rm NN}}$=5.02 TeV, Phys. Lett. B 805 (2020) 135434, 10.1016/j.physletb.2020.135434
19. J. Adam et al., J/ψ suppression at forward rapidity in Pb-Pb collisions at $\sqrt{s_{\rm NN}} = 5.02$ TeV, Phys. Lett. B 766 (2017) 212, 10.1016/j.physletb.2016.12.064
20. S. Pratt, Balance functions: A signal of late-stage hadronization, Nucl. Phys. A 698 (2002) 531, 10.1016/S0375-9474(01)01421-X
21. S. Jeon and S. Pratt, Balance functions, correlations, charge fluctuations and interferometry, Phys. Rev. C 65 (2002) 044902, 10.1103/PhysRevC.65.044902
22. J. Adams et al., Narrowing of the balance function with centrality in Au – Au collisions at $\sqrt{s_{\rm NN}} = 130$ GeV, Phys. Rev. Lett. 90 (2003) 172301, 10.1103/PhysRevLett.90.172301
23. M. M. Aggarwal et al., Balance Functions from Au+Au, d+Au, and $p + p$ Collisions at $\sqrt{s_{NN}}$ = 200 GeV, Phys. Rev. C 82 (2010) 024905, 10.1103/PhysRevC.82.024905
24. L. Adamczyk et al., Beam-energy dependence of charge balance functions from Au + Au collisions at energies available at the BNL Relativistic Heavy Ion Collider, Phys. Rev. C 94 (2016) 024909, 10.1103/PhysRevC.94.024909
25. H. Wang, Study of charge-dependent azimuthal correlations using reaction-plane-dependent balance functions, J. Phys. G 38 (2011) 124188, 10.1088/0954-3899/38/12/124188
26. B. Abelev et al., Charge correlations using the balance function in Pb-Pb collisions at $\sqrt{s_{NN}}$ = 2.76 TeV, Phys. Lett. B723 (2013) 267, 10.1016/j.physletb.2013.05.039
27. J. Adam et al., Multiplicity and transverse momentum evolution of charge-dependent correlations in pp, p–Pb, and Pb–Pb collisions at the LHC, Eur. Phys. J. C 76 (2016) 86, 10.1140/epjc/s10052-016-3915-1
28. S. Pratt and C. Plumberg, Determining the Diffusivity for Light Quarks from Experiment, Phys. Rev. C 102 (2020) 044909, 10.1103/PhysRevC.102.044909
29. S. Pratt and C. Plumberg, Charge balance functions for heavy-ion collisions at energies available at the CERN Large Hadron Collider, Phys. Rev. C 104 (2021) 014906, 10.1103/PhysRevC.104.014906
30. J. Pan, Balance functions of (un)identified hadrons in Pb–Pb, p–Pb, and pp collisions at the LHC, Nucl. Phys. A 982 (2019) 315, 10.1016/j.nuclphysa.2018.09.022
31. S. Acharya et al., General balance functions of identified charged hadron pairs of $(\pi, {\rm K}, {\rm p})$ in Pb$-$Pb collisions at $\sqrt{s_{\rm NN}} = 2.76$ TeV (2021)
32. G. Aarts, et al., Finite Temperature Lattice QCD - Baryons in the Quark-Gluon Plasma, Acta Physica Polonica B Proceedings Supplement 9 (2016), 10.5506/APhysPolBSupp.9.441